Vibration-Based Measurement of Activated Cylinders in Reciprocating Machines

Thomas C. Krause, *Graduate Student Member, IEEE*, Devin W. Quinn, Łukasz Huchel, and Steven B. Leeb, *Fellow, IEEE*

***Abstract*— Vibration signals from rotating and reciprocating machines provide insights into machine health and operating parameters. Reciprocating machines often feature cylinder deactivation systems for increased efficiency. This article presents a vibration-based method for the detection of activated cylinders in reciprocating machines. Simulated compressor vibration signals demonstrate the effect of cylinder conditions on spectral-coherence and mean-envelope-spectrum (MES) estimates. Physical parameters of the mechanical system and the results of the simulations advise the proposed method. With an appropriately chosen region of interest (ROI), the MES-based indicator (MESbI) correctly identified the number of activated cylinders of a four-cylinder reciprocating refrigeration compressor in both field and laboratory test setups. A discussion section addresses measurement uncertainty and calibration, and provides an example application.**

***Index Terms*— Cyclostationarity, mean envelope spectrum (MES), mechanical systems, reciprocating machines, signal processing, vibration analysis.**

I. Introduction

RECIPROCATING machines ushered in the industrial revolution and are still essential today. Reciprocating steam engines drove early power distribution systems [1]. Compressors are the workhorse of refrigeration and cooling systems [2], [3]. Pumps move fluids for a variety of applications [4]. Internal combustion engines propel the majority of today's vehicles. Typical reciprocating-machine system designers apply conservative sizing practices and, during normal operation, less than the maximum capacity of the machine that meets system demand. Consequently, for increased efficiency, many modern reciprocating machines offer cylinder deactivation systems. For example, in gasoline internal-combustion engines, the injection and ignition stages of the combustion cycle for certain cylinders may be skipped during periods of low demand [5]. The so-called "unloaders" deactivate reciprocating compressor cylinders based on system demand. In addition, system faults may manifest themselves as misfires or blown valves and effectively disengage cylinders [6]. Knowledge of the activated cylinders provides insight into system operation.

This work proposes a technique for determining the number of activated cylinders of reciprocating machines from their vibration signal. Applications include system monitoring and fault detection and diagnostics (FDD). Other vibration-based FDD techniques for reciprocating machines include estimating cylinder pressure, instantaneous angular speed analysis, and artificial neural networks [7], [8], [9], [10]. The choice of FDD approach depends on the specific type of machinery, available sensors, and quality of measurements. Antoni et al. [11], [12] provided one of the early applications of cyclostationary analysis for fault diagnosis of internal-combustion engines. Cyclostationary analysis of vibration signals from rotating machinery, for example, estimation of the spectral correlation or spectral coherence function, yields useful information for diagnostics and condition-based maintenance [13], [14], [15], [16]. Since initial applications of cyclostationary analysis to mechanical systems, new tools have emerged, such as the mean envelope spectrum (MES), also referred to in the literature as the improved envelope spectrum, which is an envelope-analysis tool calculated from the spectral coherence function [4], [17], [18], [19]. This article shows a new application of vibration analysis with the MES and associated indicators. The physics of the machine informs the signal processing approach. Contributions of this work include simulations with signal models constructed from first principles and details of the mechanical system of interest. The simulation results provide intuition for the cyclostationary signal processing tools. An experimental study with reciprocating refrigeration compressors verifies the simulation results and demonstrates an application of the proposed technique. The method presented in this article can be applied to other types of reciprocating machines with different parameters.

The outline of the work is given as follows. Section II reviews cyclostationary signal processing. Section III describes the reciprocating machine of interest. Section IV discusses simulated vibration signals motivated by the physical parameters of the system. Cyclostationary signal processing tools process the simulated signals. Section V provides motivating experimental examples for MES analysis. Section VI discusses indicators based on the MES. Section VII presents experimental results for field and laboratory test setups. Finally,

Manuscript received 23 July 2022; revised 2 October 2022; accepted 12 October 2022. Date of publication 28 October 2022; date of current version 12 January 2023. This work was supported in part by the Office of Naval Research Structural Acoustics Program and in part by The Grainger Foundation. The Associate Editor coordinating the review process was Yang Song. *(Corresponding author: Thomas C. Krause.)*

Thomas C. Krause and Steven B. Leeb are with the Department of Electrical Engineering and Computer Science, Massachusetts Institute of Technology, Cambridge, MA 02139 USA (e-mail: tkrause@mit.edu; sbleeb@mit.edu).

Devin W. Quinn is with the United States Coast Guard, Alameda, CA 94501 USA (e-mail: dwquinn@mit.edu).

Łukasz Huchel is with Enphase Energy, Austin, TX 78758 USA.

Digital Object Identifier 10.1109/TIM.2022.3218038

Section VIII discusses measurement uncertainty and considers the practical implementation of the proposed method.

II. Cyclostationary Signal Processing

Vibration signals from reciprocating and rotating machinery contain second-order periodicities that are hidden from traditional spectral analysis techniques [14], [20], [21]. Traditional techniques generally assume stationary deterministic signal models, where signals have discrete frequency components and are characterized by a Fourier series representation. Cyclostationary signal models treat signals as specific realizations of cyclostationary random processes and account for second-order periodicity. Often, cyclostationary signal models more accurately describe the underlying physics of reciprocating and rotating machine vibration [14].

Second-order periodic phenomena exhibit nonzero temporal correlation between spectral components of the time series [20]. In mechanical systems, second-order periodicities arise due to the modulation of random (broadband) vibration content by essential actions, such as reciprocation and rotation [14], [20]. The idealized spectral correlation function, also referred to as the limit cyclic spectrum, is defined as

$$\hat{S}_x^{\alpha}(f) = \lim_{T\to+\infty}\lim_{\Delta t\to+\infty}\frac{1}{\Delta t}\frac{1}{T} \times \int_{-\Delta t/2}^{\Delta t/2} X\left(u, f+\frac{\alpha}{2}\right)_T \cdot X^*\left(u, f-\frac{\alpha}{2}\right)_T du \quad (1)$$

where the subscript x denotes that this is the spectral correlation function for some signal $x(t)$, f is the carrier or center frequency in Hz, α is the cyclic frequency in Hz, $X(t, f)_T$ is a time-variant finite-length Fourier transform of $x(t)$, T is the window length, and u is a dummy variable of integration [20], [22]. Equation (1) is an idealized or limit quantity because, in practice, the measurement window length T and the averaging window length Δt are finite. This work uses quantities based on estimates of (1) from measured data. An interpretation of (1) is a spectral density of a temporal correlation between time-variant spectra where α is the lag variable. For $\alpha = 0$, the spectral correlation function is equal to the traditional power spectral density (PSD).

Vibration signatures from reciprocating machines contain many signal components of varying energy levels. To highlight component behavior instead of absolute energy level, the spectral coherence function $\gamma_x^{\alpha}(f)$ is defined as

$$\gamma_x^{\alpha}(f) = \frac{\hat{S}_x^{\alpha}(f)}{\sqrt{\hat{S}_x^{0}\left(f-\frac{\alpha}{2}\right)\hat{S}_x^{0}\left(f+\frac{\alpha}{2}\right)}}. \quad (2)$$

The spectral coherence function is the spectral correlation function normalized by a function of values from the PSD. The spectral coherence is a measure of cyclostationarity [20], [21].

In general, the spectral coherence function is a complex-valued function of two independent variables. A compressed quantity that highlights the important features of the spectral coherence magnitude is of interest. To address this, the MES [4] $S_x^{\langle f\rangle}(\alpha)$ over some range of carrier frequencies $F = [f_{\text{low}}, f_{\text{up}}]$ is defined as

$$S_x^{\langle f\rangle}(\alpha) = \frac{1}{|F|}\int_F \left|\gamma_x^{\alpha}(f)\right| df \quad (3)$$

where F is chosen by the analyst and the upper bound of F is limited to one-half of the sampling frequency (Nyquist frequency) [21]. The MES collapses the 3-D spectral coherence magnitude map into a 2-D quantity. Quantities calculated from the MES are used throughout this work for the measurement of activated cylinders of a reciprocating refrigeration compressor.

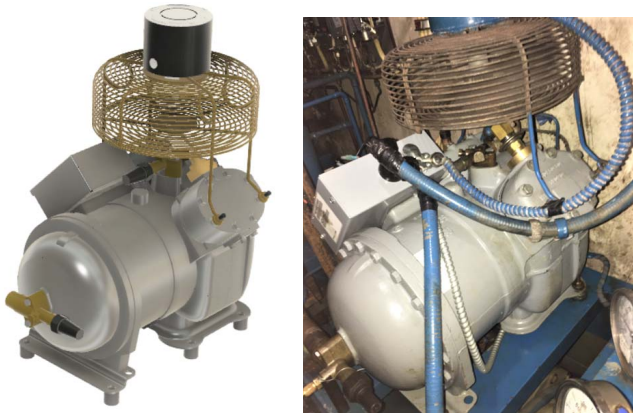

(a) (b)

Fig. 1. Carlyle model 06D four-cylinder compressor: (a) CAD model [23] and (b) low-temperature refrigerant compressor onboard CG vessel.

III. Reciprocating Machine System

Cyclostationary signal processing, specifically cyclic spectral analysis, enables the investigation of hidden (second-order) periodicities in machine vibration signals. Where to look in the cyclic spectrum, spectral coherence, or MES to obtain insights into machine operating conditions is system-dependent. This section presents the details of the example reciprocating machine system necessary to formulate cyclic-spectrum-based indicators of activated cylinders. Section IV explores the spectral coherence and MES for simulated compressor vibration signals.

A. Compressor Operation

As an example, this article demonstrates cyclostationary signal processing applied to vibration measurements of a Carlyle 06D semi-hermetic reciprocating compressor. The Carlyle model 06D studied in this paper is a four-cylinder single-stage single-acting compressor, meaning all four cylinders discharge to the same manifold and only the head side of the cylinder preforms compression. Fig. 1(a) shows a CAD model of the compressor reproduced from [23]. Fig. 1(b) shows a picture of the compressor in a low-temperature refrigerant setup onboard a United States Coast Guard (CG) vessel. This type of compressor is typically connected to a refrigeration system that includes thermal expansion valves, evaporators, condensers, and associated piping. In broad terms, refrigeration systems use the phase transitions of a refrigerant to transfer heat and control the environmental conditions of

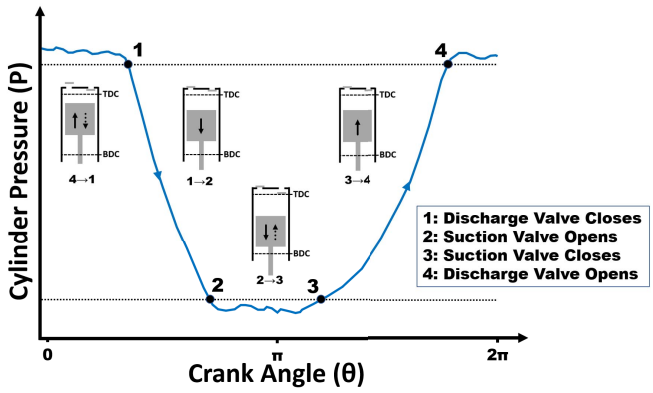

Fig. 2. Pressure versus crank angle plot (one-cylinder of compressor).

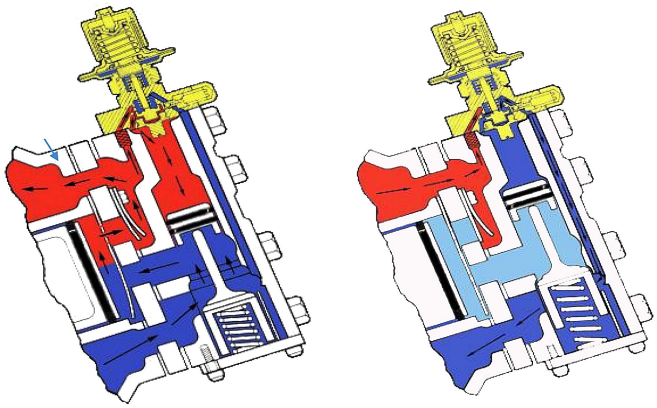

(a) (b)

Fig. 3. Pressure-actuated suction-cutoff unloader [25]: (a) loaded operation and (b) unloaded operation.

a space. Compressors enable the heat-transfer process and provide energy to the refrigeration system by converting cold low-pressure refrigerant to superheated vapor.

During the operation of the Carlyle model 06D compressor, an induction machine enclosed in the compressor housing rotates the crankshaft of the compressor. Four connecting rods join four pistons to the crankshaft, and as the crankshaft rotates, the pistons reciprocate in the cylinders from the top dead center (TDC) to the bottom dead center (BDC). TDC corresponds to the minimum cylinder volume, and BDC corresponds to the maximum cylinder volume. The changes in cylinder volume and pressure actuate suction and discharge valves. Cylinders draw-in refrigerant through suction valves and discharge refrigerant through discharge valves. Fig. 2 shows a theoretical pressure versus crank angle plot of a single cylinder of the compressor. The upper dotted line represents discharge pressure, and the lower dotted line represents suction pressure. As the piston travels toward BDC, cylinder pressure decreases below suction pressure, and the suction valve opens (point 2). As the piston travels toward TDC, cylinder pressure increases above discharge pressure, and the discharge valve opens (point 4). Activated cylinders pull refrigerant through suction ports and discharge compressed refrigerant to the high-pressure side of the system. This compression cycle repeats for each activated cylinder every crankshaft rotation [24].

B. Suction Cutoff Unloaders

The compressor has two operating states: two activated cylinders and four activated cylinders. A capacity control valve installed on one head (cylinder pair) of the Carlyle 06D compressor activates cylinders based on cooling demand. The other head does not have an unloader, and the cylinders are always activated. During periods of high demand, the capacity control valve activates more cylinders. The two-cylinder state is referred to as "unloaded operation" and the four-cylinder state is referred to as "loaded operation." Consequently, capacity control valves are commonly referred to as unloaders.

Fig. 3 presents diagrams of a Carlyle 06D compressor head with a suction-cutoff unloader. Fig. 3(a) depicts the loaded operation, and Fig. 3(b) depicts the unloaded operation. The diagrams are from [25]. A suction-cutoff unloader blocks or "cuts off" the suction port and deactivates both cylinders inside of a head. This pressure-actuated suction-cutoff unloader is activated by discharge pressure and controlled by suction pressure. The unloader is the topmost structure and contains a diaphragm, valves, orifices, springs, and control set point adjustment nut. The position (number of turns) of the control set point adjustment nut determines the pressures at which the unloader activates and deactivates cylinders. The discharge pressure is the shaded area in the upper left, and the suction pressure is the shaded area in the bottom right. In Fig. 3(b), cylinder pressure during unloaded operation is the lighter shaded area in the middle. When the suction-pressure force applied to the unloader diaphragm overcomes the spring forces, the poppet valve allows discharge gas to compress the unloader valve spring. This opens the suction port for loaded operation [25]. When the spring forces applied to the unloader diaphragm overwhelm the suction-pressure force, the poppet valve vents discharge gas to the cylinder's suction side for unloaded operation. The unloader valve spring extends, and the suction port is "cutoff" from the suction valve.

Unloaders deactivate cylinders during periods of low cooling demand and reduce the power consumption of the compressor. However, if an unloader load point is too high, the compressor runs perpetually unloaded and never satisfies higher cooling demands. The cylinders in the head without an unloader naturally wear at an increased rate due to more cumulative compression cycles. However, an improperly set unloader accentuates the disparity and can lead to early equipment failure. If an unloader load point is too low, it may run perpetually loaded. This will likely satisfy all cooling demands but at an increased risk of liquid floodback to the compressor. Liquid floodback occurs when refrigerant does not fully transition to its gaseous state in the evaporator and liquid refrigerant returns to the compressor. The liquid refrigerant is incompressible and can result in catastrophic damage to the compressor. Proper operation of capacity control devices is crucial for system efficiency and extended compressor lifetime [24].

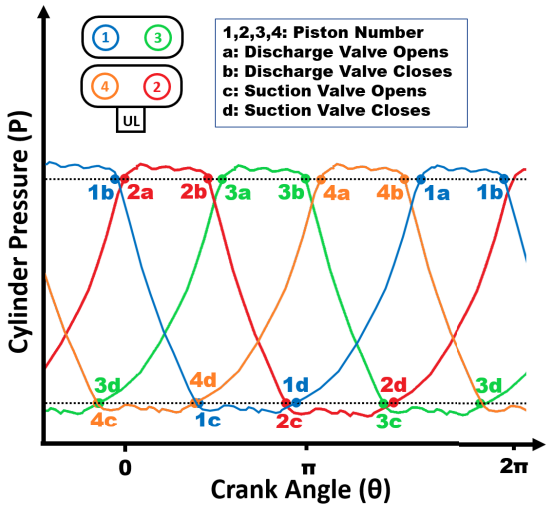

Fig. 4. Pressure versus crank angle plot (four-cylinder compressor) [24].

C. Compressor Vibration

The compression cycle in Fig. 2 repeats during each shaft rotation. With multiple pistons, this cycle remains the same, but there is a symmetric phase shift in the crank angle for each cylinder's compression cycle. Fig. 4 shows a theoretical pressure versus crank angle plot of a Carlyle 06D with four activated cylinders (loaded operation).

The vibration signature of reciprocating machines is rich in frequency content. Lower frequency vibration is typically associated with mechanical events that occur throughout shaft rotation and can be a result of imbalance or looseness within the machine. Higher frequency content is likely the result of valve action, turbulent gas flow, and excitation of the compressor's internal natural frequencies [26]. Suction and discharge valves open and close periodically throughout shaft rotation when cylinder pressure equalizes with the system pressure of the applicable side, that is, the high-pressure side for discharge valves and the low-pressure side for suction valves. The pressure gradient induced during the opening and closing of discharge valves and during the opening of suction valves is typically large enough to produce impulses visible in the time domain of the vibration signature [24]. The closing of suction valves is less violent and not normally apparent in the vibration signature. During loaded operation, the vibration signal is generally modulated four times per shaft rotation. During the unloaded operation, frequency content is generally modulated two times per shaft rotation.

IV. Cataloging Vibration Signals

This section presents simulated compressor vibration signals. The signal models incorporate Carlyle 06D parameters and operating specifications, such as the number of cylinders and shaft rotational speed. Section IV-A uses evenly modulated white-noise signals as a simple model for compressor vibration. Section IV-B uses unevenly modulated and periodically filtered white-noise signals as a more-realistic model for compressor vibration. Section IV-C introduces modulated high-frequency signals to the vibration signal model

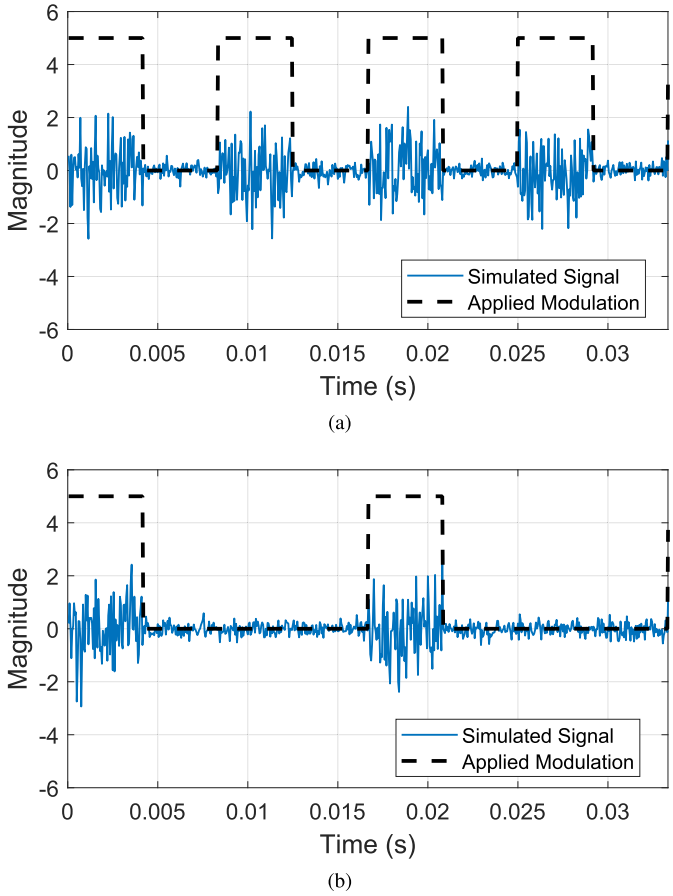

Fig. 5. Simulated vibration signals: (a) pulsed white-noise signal to simulate loaded operation and (b) pulsed white-noise signal to simulate unloaded operation.

of Section IV-B. Cyclostationary signal processing techniques process the simulated signals. The results provide intuition and guide the development of indicators for the detection of activated cylinders of a reciprocating compressor in the experimental scenarios presented in Section VII. Techniques in this section are applicable to other reciprocating machines with adjustments for application-specific parameters.

A. Broadband Signals and Even Modulation

Pulsed white noise signals served as a first-order approximation of compressor vibration. The MATLAB function *randn()* generated 240 000 realizations of a normally distributed random variable. The realizations formed a white-noise signal with a 12-s-long measurement time and 20-kHz sampling rate. Two of these random signals were created. The white-noise signals were then modulated by a square-wave signal, one corresponding to loaded operation, and one corresponding to the unloaded operation. The loaded modulation signal represented the four compression strokes of a loaded compressor with four pulses per shaft rotational period. The unloaded modulation signal represented the two compression strokes of an unloaded compressor with two pulses per shaft rotational period. Both square-wave modulation signals had a magnitude of five when "ON" and a magnitude of zero when "OFF." The rated shaft rotational speed of the Carlyle 06D compressor is

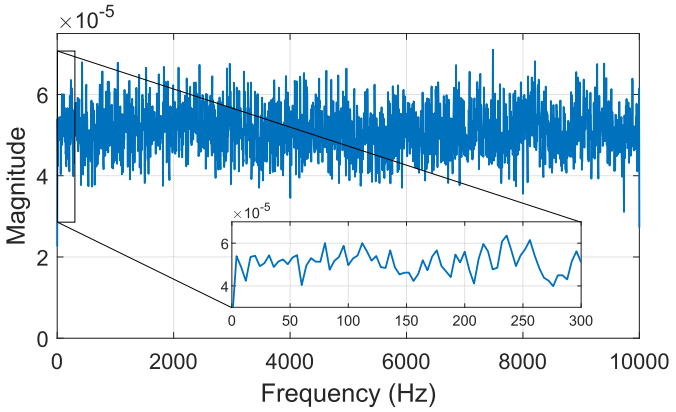

Fig. 6. PSD of the loaded pulsed white-noise signal.

29.17 revolutions per second (rps), but the signal models used 30 rps for simplicity. Finally, to ensure that there was signal content during the "OFF" periods, an unmodulated white-noise signal normalized such that the maximum/minimum was equal to ± 1 was also added to each signal. Fig. 5(a) and (b) shows shaft periods of the simulated loaded and unloaded compressor vibration signals, respectively. The dashed lines are the applied modulation, and the solid lines are the simulated signals.

Fig. 6 shows an estimate of the PSD for the signal in Fig. 5(a). The Welch method of averaging modified periodograms generated the estimate [22]. The method used a Hamming window of 0.25 s (5000 samples) and 50% overlap of signal segments. There is no indication of periodicity, i.e., no distinct peaks in the PSD estimate. Besides inherent variation associated with signal generation and computation, the estimate is constant in frequency and agrees with the frequency-independent PSD of theoretical white noise [20], [22]. The 120-Hz periodicity of the simulated loaded signal is hidden.

There is a closed-form expression for the magnitude of the spectral coherence function of pulsed white noise signals; Gardner derives the result in [20]. The expression is in terms of the Fourier series coefficients of the periodic modulation signal. The Fourier series representation of a signal $x(t)$ is given by the synthesis equation

$$x(t) = \sum_{k=-\infty}^{+\infty} a_k e^{jk2\pi f_0 t} \tag{4}$$

and the analysis equation

$$a_{kf_0} = \frac{1}{T}\int_T x(t) e^{-jk2\pi f_0 t} dt \tag{5}$$

where k is the harmonic order, T is the fundamental period, and $f_0 = 1/T = \omega_0/(2\pi)$ is the fundamental frequency in Hz. The subscripts of the Fourier coefficients in (5) denote the frequencies of the complex exponentials in Hz. For pulsed white noise, the magnitude of the spectral coherence is

$$\left|\gamma_x^{\alpha}(f)\right| = \frac{\left|\sum_{k=-\infty}^{+\infty} a_{kf_0} a_{\alpha - kf_0}\right|}{\sum_{k=-\infty}^{+\infty} \left|a_{kf_0}\right|^2} \tag{6}$$

where k is the harmonic order and a_{kf_0} are the Fourier Series coefficients of the periodic modulation signal. The right-hand side of (6) is independent of frequency because the underlying signal is broadband.

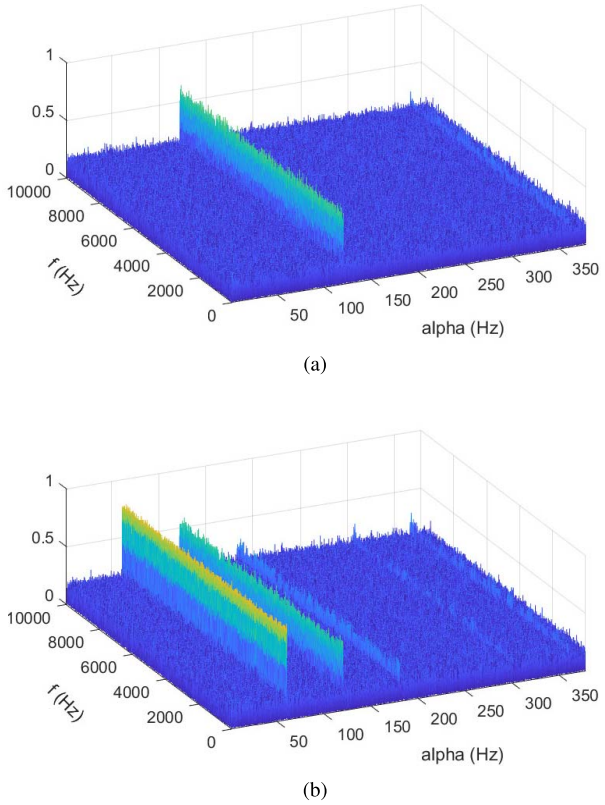

Fig. 7. Spectral coherence magnitude maps of simulated pulsed white-noise vibration signals: (a) loaded compressor and (b) unloaded compressor.

For a square wave with fundamental period T and duty cycle D, from (5), the Fourier coefficients are

$$a_{kf_0} = \frac{\sin\left(\frac{kf_0\pi D}{f_0}\right)}{k\pi} \tag{7}$$

for $k = (-\infty, +\infty)$, $k \neq 0$. The modulation of the simulated loaded signal shown in Fig. 5(a) has a dc offset of (1/2), $f_0 = 120$ Hz, and $D = 0.5$ [27]. The Fourier coefficients for $k = [-3, 3]$ of the modulation are

$$\begin{aligned} a_{0\text{ Hz}} &= \frac{1}{2} \\ a_{\pm 120\text{ Hz}} &= \frac{1}{\pi} \\ a_{\pm 360\text{ Hz}} &= \frac{-1}{3\pi} \\ a_{\pm 600\text{ Hz}} &= \frac{1}{5\pi}. \end{aligned} \tag{8}$$

Computation of (6) for $\alpha = [0, 360]$ with (10) yields

$$\begin{aligned} \left|\gamma_x^{\alpha=0\text{ Hz}}(f)\right| &= 1 \\ \left|\gamma_x^{\alpha=120\text{ Hz}}(f)\right| &= \frac{2}{\pi} \approx 0.6366 \\ \left|\gamma_x^{\alpha=360\text{ Hz}}(f)\right| &= \frac{2}{3\pi} \approx 0.2122. \end{aligned} \tag{9}$$

Fig. 7(a) presents an estimate of the spectral coherence magnitude map of the simulated loaded compressor vibration

signal in Fig. 5(a). The fast spectral correlation algorithm estimated the spectral coherence [28]. The case of $\alpha = 0$ is not shown because $\alpha \neq 0$ is of interest. There are spectral lines at $\alpha = 120$ and 360 Hz. For these values of α, across all carrier frequencies f, the spectral coherence magnitudes are approximately those listed in (9).

The modulation of the simulated unloaded signal shown in Fig. 5(b) has a dc offset of $(1/2)$, $f_0 = 60$ Hz, and $D = 0.25$ [27]. The Fourier coefficients for $k = [-5, 5]$ of the modulation are

$$\begin{aligned} a_{0\text{ Hz}} &= \frac{1}{2} \\ a_{\pm 60\text{ Hz}} &= \frac{\sqrt{2}}{2\pi} \\ a_{\pm 120\text{ Hz}} &= \frac{1}{2\pi} \\ a_{\pm 180\text{ Hz}} &= \frac{\sqrt{2}}{3\pi} \\ a_{\pm 240\text{ Hz}} &= 0 \\ a_{\pm 300\text{ Hz}} &= \frac{-\sqrt{2}}{10\pi}. \end{aligned} \tag{10}$$

Computation of (6) for $\alpha = [0, 360]$ with (10) yields

$$\begin{aligned} \left|\gamma_x^{\alpha=0\text{ Hz}}(f)\right| &= 1 \\ \left|\gamma_x^{\alpha=60\text{ Hz}}(f)\right| &\approx 0.7717 \\ \left|\gamma_x^{\alpha=120\text{ Hz}}(f)\right| &\approx 0.5457 \\ \left|\gamma_x^{\alpha=180\text{ Hz}}(f)\right| &\approx 0.2573 \\ \left|\gamma_x^{\alpha=300\text{ Hz}}(f)\right| &\approx 0.1543 \\ \left|\gamma_x^{\alpha=360\text{ Hz}}(f)\right| &\approx 0.1819. \end{aligned} \tag{11}$$

Fig. 7(b) presents an estimate of the spectral coherence magnitude map of the simulated unloaded compressor vibration signal in Fig. 5(b). There are spectral lines at $\alpha = 60, 120, 180, 300$, and 360 Hz. For these values of α, across all carrier frequencies f, the spectral coherence magnitudes are approximately those listed in (11).

The MES provides a 2-D view of average quantities from the spectral coherence magnitude map. Fig. 8(a) and (b) shows the MESs for the loaded and unloaded simulated signals, respectively. For these plots, the integration range $F = [0, 10\text{ kHz}]$. For these cases, the spectral coherence magnitude is independent of frequency, and the MES values are equal to the spectral coherence magnitudes given in (9) and (11).

The simulated signals are first-order approximations of measured vibration signals of a compressor operating with four and two activated cylinders, respectively. For the simulated loaded compressor vibration signal, there are four actions per shaft rotation, and the fourth-order cyclic frequency of the MES is dominant. For the simulated unloaded compressor vibration signal, there are two actions per shaft rotation, and the second-order cyclic frequency of the MES is dominant. These signals model compressor vibration as totally broadband and modulated evenly by each cylinder. In practical compressor vibration signals, there are narrowband components from rotation, and all components are shaped by system responses, typically characterized by resonant peaks. In addition, each

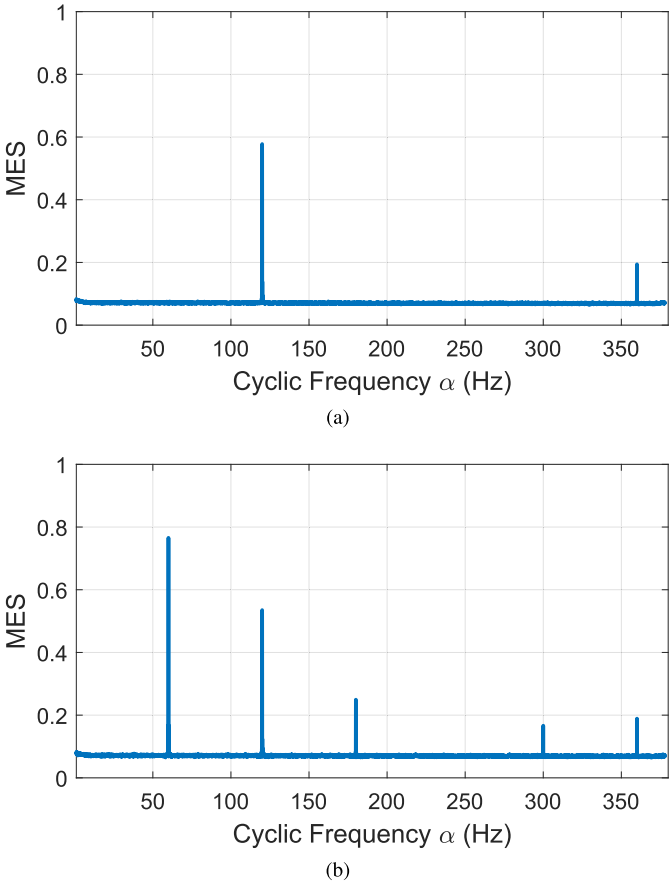

Fig. 8. MES of the simulated pulsed white-noise vibration signals: (a) loaded compressor and (b) unloaded compressor.

cylinder may apply a different level of modulation due to manufacturing or installation differences and cylinder-specific wear or appear to be because of accelerometer mounting location. The effect of uneven, cylinder-specific responses and uneven modulation is explored in Section IV-B.

B. Uneven Resonances and Uneven Modulation

The section explores the spectral coherence magnitude and corresponding MES for a simulated loaded compressor vibration signal with uneven system resonant frequencies and uneven modulation magnitudes. Considered separately, both uneven frequency responses due to specific cylinder excitation, that is, some transfer function, such as a second-order resonant peak that shapes the excitation, and modulation magnitude for each activated cylinder produce MES peaks at the shaft rotational frequency at its harmonics. For example, if the applied modulation in Fig. 5(a) had a fundamental period equal to a shaft rotation, its Fourier series would give rise to MES peaks at the first, second, third, and so on order cyclic frequencies described by (6) and not just the fourth-order cyclic frequency. Uneven frequency responses with even modulation produce a similar result. The relative magnitudes of the MES peaks are dependent upon the relative "unevenness" or "symmetry" of the frequency responses and modulation. The combination of uneven responses and modulation magnitudes is found in practice and is a better model for measured reciprocating machine

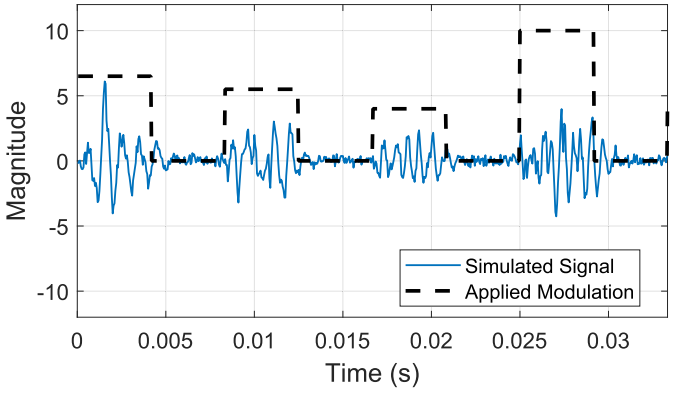

Fig. 9. Simulated vibration signal of a loaded compressor with uneven responses and uneven modulation.

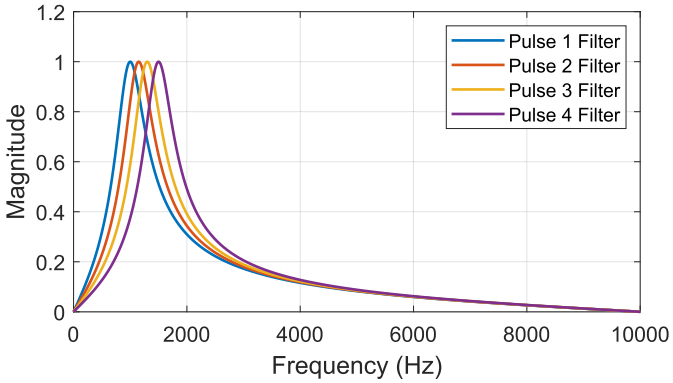

Fig. 10. System frequency response (filter) for each pulse.

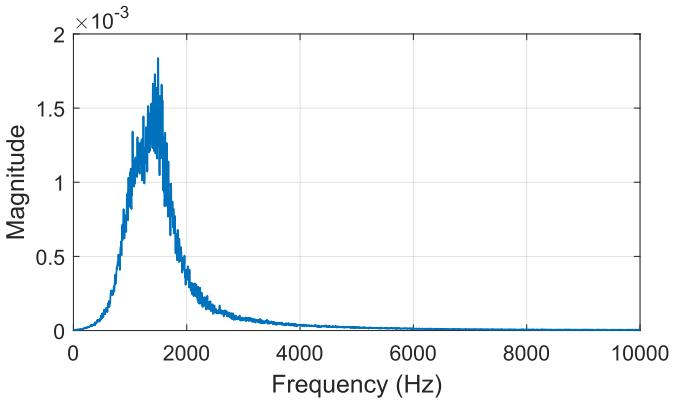

Fig. 11. PSD of the simulated vibration signal of a loaded compressor with uneven responses and uneven modulation.

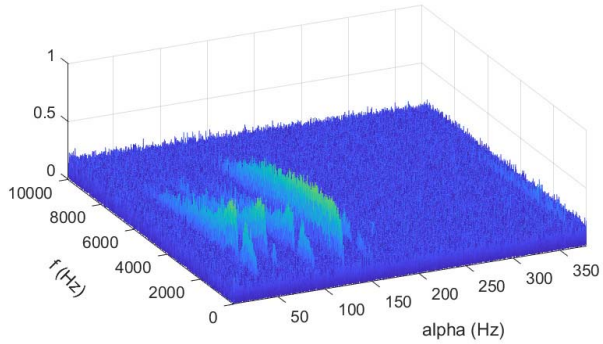

Fig. 12. Spectral coherence magnitude map of the simulated vibration signal of a loaded compressor with uneven responses and uneven modulation.

vibration signals compared to totally broadband pulsed white noise. Each activated cylinder modulates vibration content with its own magnitude. Each cylinder has characteristics and excites structural resonances that are distinct from the other cylinders. For a healthy machine, the differences may be small, but no system is perfectly balanced or symmetric.

Fig. 9 shows a shaft period of a simulated loaded compressor vibration signal with unique modulation magnitudes and resonant frequencies. A process similar to that described in Section IV-A created the signal, but the frequency-dependent signal model in this section necessitated additional filtering steps. The pulses of the square-wave modulation signals had magnitudes of 6.5, 5.5, 4.0, and 10.0 (magnitudes of 1.3, 1.1, 0.8, and 2 relative to 5), respectively. The products of the random signal and four pulses created four separate signals. At this point, each signal was scaled white noise during its corresponding pulse and zero otherwise. Then, second-order resonant filters with resonant frequencies of 1, 1.15, 1.3, or 1.5 kHz, respectively, filtered the signals. Fig. 10 shows the filters for each pulse. Finally, the signals were added together and then added with a white-noise signal normalized such that the maximum/minimum value of the noise was equal to ± 1. The more-frequent zero crossings in the last pulse indicate higher frequency signal content and the higher frequency peak present in its filter. Fig. 11 presents an estimate of the PSD of the signal in Fig. 9. The Welch method produced the estimate, as described in Section IV-A. The PSD reveals the distribution of signal power across frequency, and here, power is mostly concentrated around the peaks of the filters (1–1.5 kHz). There is no indication of the periodicity at 30, 60, 90, or 120 Hz.

In Section IV-A, the simulated signal was broadband. In this section, the simulated signal has varying signal power over frequency. A discussion about filtering and cyclic spectra is necessary. For linear time-invariant (LTI) transformations, such as a filter characterized by an impulse response $h(t)$, the input and output to the filter are related by convolution

$$y(t) = \int_{-\infty}^{+\infty} h(t-u)x(u)du. \tag{12}$$

The relationship between the spectral correlation of $x(t)$ and $y(t)$ is given by

$$\hat{S}_y^\alpha(f) = H\left(f + \frac{\alpha}{2}\right) H^*\left(f - \frac{\alpha}{2}\right) \hat{S}_x^\alpha(f) \tag{13}$$

and the spectral coherence, γ, is still described by (2) [20]. Generally, filtering affects the spectral correlation and, for $\alpha = 0$, resolves to the familiar case that relates the PSD of the input and output of an LTI system. However, the simulated signal here is modulated and filtered in a progression that repeats periodically every shaft rotation. This is a linear periodically time-variant (LPTV) transformation. Gardner provides a general treatment of cyclic spectra generated by LPTV transformations of stationary time series in [20]. If known, LTI and LPTV transformations have predictable impacts on spectral correlation, coherence, and MES.

Fig. 12 shows the spectral coherence magnitude estimate of the simulated loaded compressor vibration signal in Fig. 9.

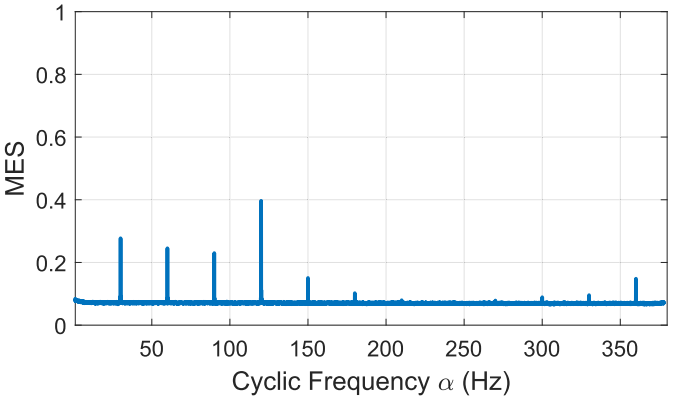

Fig. 13. MES of the simulated vibration signal of a loaded compressor with uneven responses and uneven modulation.

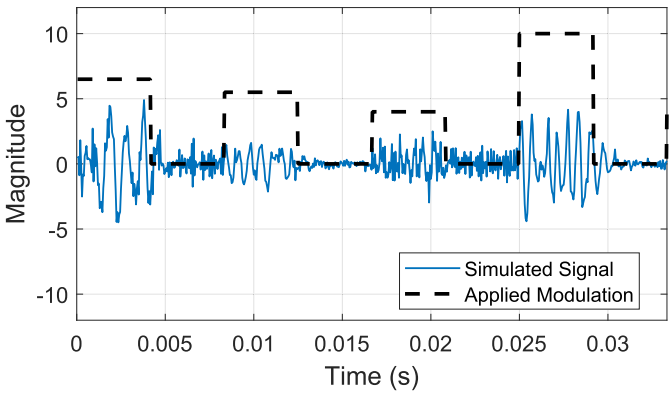

Fig. 14. Simulated vibration signal of a loaded compressor with uneven responses, uneven modulation, and added high-frequency content.

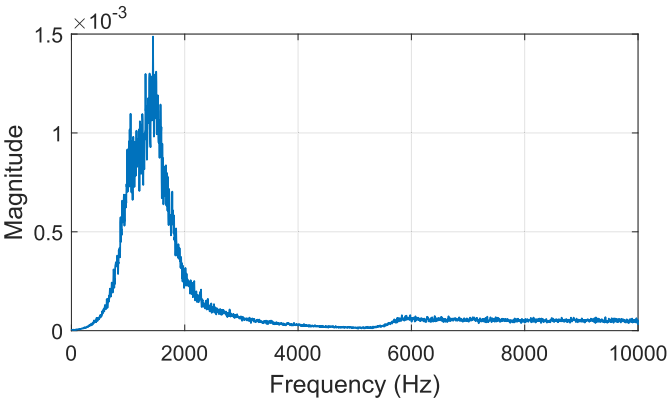

Fig. 15. PSD of the simulated vibration signal of a loaded compressor with uneven responses, uneven modulation, and added high-frequency content.

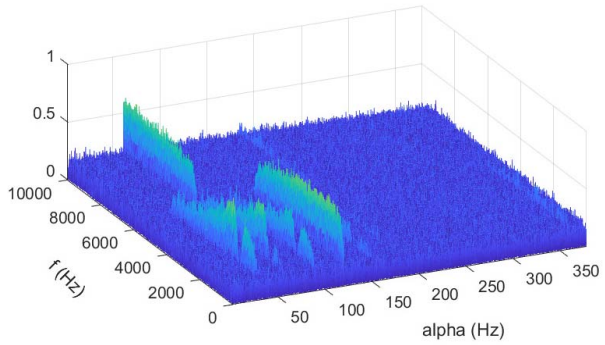

Fig. 16. Spectral coherence magnitude map of the simulated vibration signal of a loaded compressor with uneven responses, uneven modulation, and added high-frequency content.

The spectral coherence magnitude is nonzero for $\alpha = 30$ Hz and its harmonics. The system responses and modulation signal are periodic once per shaft rotation and cause nonzero spectral coherence at the first-order cyclic frequency. The spectral coherence has an interesting dependence on frequency f due to the filtering of the pulses.

Fig. 13 presents the MES of the simulated loaded compressor vibration signal with $F = [0, 10\text{ kHz}]$. There are peaks at the first-, second-, and third-order cyclic frequencies. In this case, despite the uneven responses and modulation, the insights gained from Section IV-A hold, and the fourth-order MES peak is dominant. Note that the MES does not retain information about the specific dependence of the spectral coherence on f. Section IV-C illustrates the importance of the frequency range F of the MES.

C. Uneven Resonances, Uneven Modulation, and Added High-Frequency Content

In mechanical systems, different actions have unique vibration signatures. For example, the vibration of rotating machines is typically composed of the rotational frequency component and its harmonics. Rolling-element bearings create vibration signatures with ball-pass frequency components. Systems with a turbulent fluid flow have more broadband vibration. Often, these phenomena occur periodically and correspond with fundamental actions, such as rotation or reciprocation. This section investigates the effect of high-frequency vibration content that occurs twice per shaft rotation on the MES and shows that the proper choice of F can maximize insight from the MES.

Fig. 14 shows a shaft period of a simulated loaded compressor vibration signal with unique modulation magnitudes and resonant frequencies. The signal model of Section IV-B constructed the signal in Fig. 14, but the signal also contains an additional high-frequency signal modulated twice per shaft rotation. A white-noise signal filtered by a minimum-order digital filter with a passband frequency of 6 kHz and a stopband attenuation of 60 dB produced the high-frequency signal. High-frequency content is visible between third and fourth pulses. Fig. 15 presents an estimate of the PSD of the simulated loaded compressor vibration signal. The Welch method produced the estimate, as described in Section IV-A. The majority of the signal power is concentrated around 1–1.5 kHz, but there is a noticeable increase around 6 kHz.

Fig. 16 shows the spectral coherence magnitude estimate of the simulated loaded compressor vibration signal. Below $f = 6$ kHz, the contours of the magnitude plot are almost identical to the spectral coherence magnitude estimate shown in Fig. 12. The spectral coherence is nonzero at $\alpha = 60, 180, 300$ Hz for $f > 6$ kHz. These contributions are due to the high-frequency content that repeats twice per shaft rotation. Although the high-frequency content was additive, the spectral coherence (see (2)) is a nonlinear expression, and superposition of the

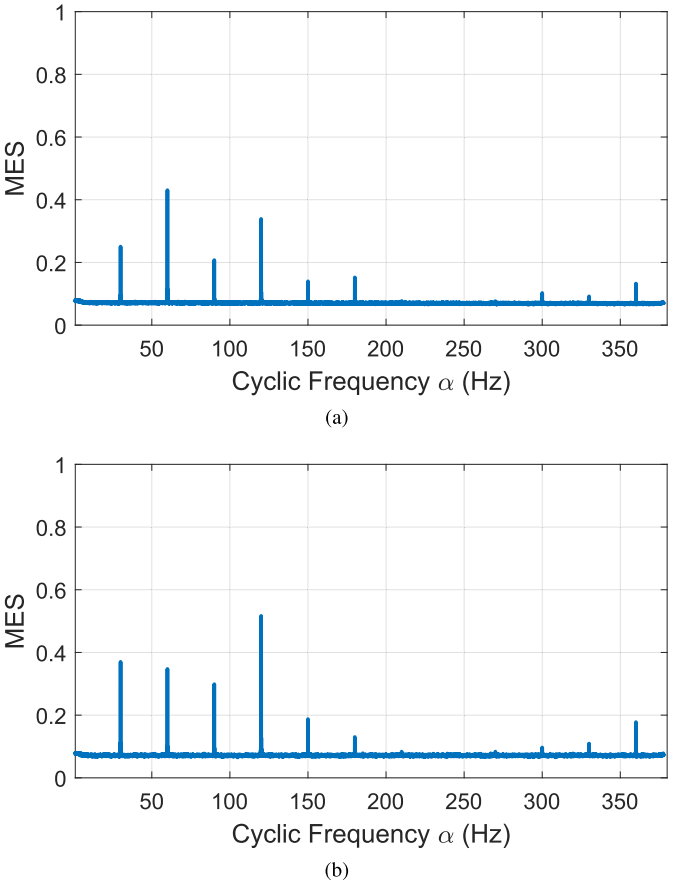

Fig. 17. MES with different F's of the simulated vibration signal of a loaded compressor with uneven responses, uneven modulation, and added high-frequency content: (a) $F = [0, 10\ \text{kHz}]$ and (b) $F = [0, 6\ \text{kHz}]$.

spectral coherence maps does not hold between this simulation and the simulation of Section IV-B. Periodic high-frequency content could be a model for valve action in a reciprocating compressor.

The MES loses information on how the spectral coherence magnitude varies with carrier frequency f. Fig. 17(a) presents the MES of the simulated signal with frequency range $F = [0, 10\ \text{kHz}]$. The second-order cyclic frequency component is the dominant component of the MES. This is unexpected. The signal simulates a loaded compressor with four activated cylinders, which, in previous simulations, produced a dominant fourth-order peak. The higher frequency content that occurs two times per shaft rotation masks the expected MES result. A properly chosen F recovers the dominant fourth-order peak. Fig. 17(b) shows the MES of the simulated signal with the frequency range of $F = [0, 6\ \text{kHz}]$. The fourth-order cyclic frequency component is now the dominant component in the MES. This example illustrates the importance of the integration frequency range of the MES and advises the analysis of Section VII.

V. Motivating Examples

This section presents experimental data from other reciprocating machines. The results resemble the simulated signals in Section IV and further motivate the investigation of the relative magnitudes of MES orders. Section VII presents an experimental study of MES order-based activated cylinder measurement of a reciprocating compressor.

Fig. 18. Quincy QR-25 model number 325 two-stage compressor.

A. Two-Cylinder Two-Stage Start Air Compressor

Fig. 18 shows a picture of the start air compressor, a two-cylinder two-stage Quincy QR-25 Model Number 325, onboard a CG vessel. Two- or dual-stage compressors compress the working fluid, in this case, air, two times between the compressor inlet and discharge to the storage tank. Applications with higher system pressures often employ multistage compressors. Typically, a larger low-pressure cylinder provides the first stage of compression and a smaller high-pressure cylinder provides the second stage of compression.

A data acquisition unit connected to an accelerometer mounted on the outer housing of the compressor measured the vibration of the compressor in steady-state operation. The measurement was 12 s long and sampled at 20.833 kHz. The flask (storage tank) pressure was 230 psi. Fig. 19(a) shows the spectral coherence magnitude of the vibration measurement. An induction motor with a rated speed of 1725 rpm drove the compressor via pulleys and a belt. The motor pulley and compressor pulley had a ratio of about 3:1, and lines in the spectral coherence map appear at integer multiples of about 10.5 Hz. The first order presents the highest spectral coherence across most carrier frequencies f. Fig. 19(b) presents the MES calculated over all carrier frequencies. As expected from the spectral coherence map, the first order is dominant. The large first order does not match the number of activated cylinders but still agrees with the physics of the compressor. The two-stage operation and unsymmetrical cylinder arrangement likely create a vibration signature with second-order periodicities that most significantly repeat every shaft rotation and give rise to a dominant first order. This provides motivation for a more in-depth study of this machine, such as operation with different system pressures and different accelerometer mounting locations.

B. Six-Cylinder Air-Conditioning Compressor

Fig. 20 shows a picture of the 1-A air-conditioning compressor, a six-cylinder single-stage Carlyle 06E, onboard a CG

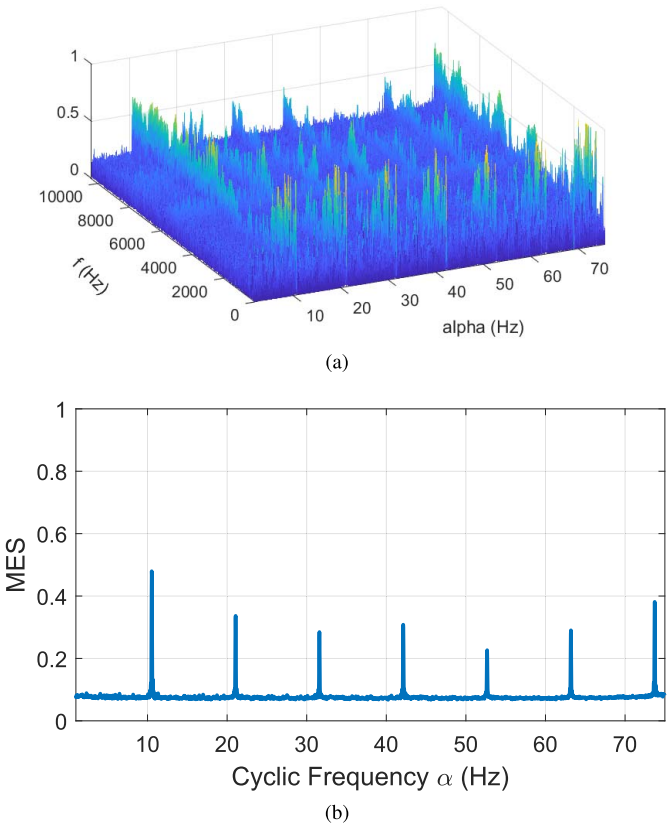

(a)

(b)

Fig. 19. Start air compressor measurements: (a) spectral coherence magnitude estimate and (b) MES.

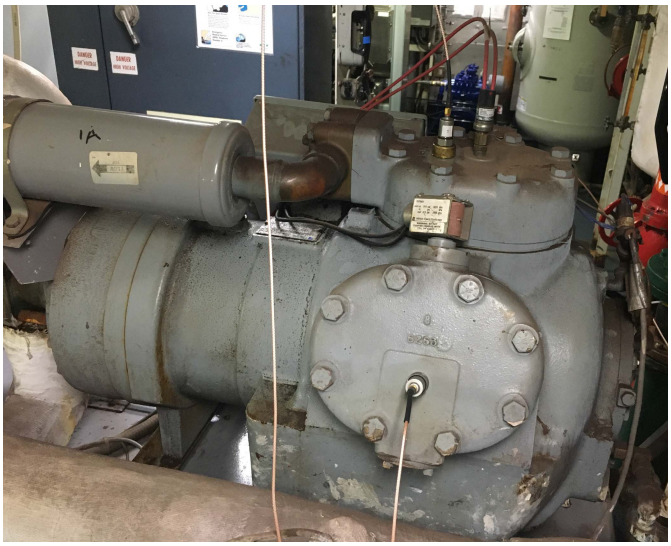

Fig. 20. Carlyle 06E six-cylinder compressor onboard CG vessel.

vessel. The Carlyle 06E in this demonstration is very similar to the Carlyle 06D, but the 06E has three heads (cylinder pairs). In the loaded operation, all six cylinders compress refrigerant.

A data acquisition unit connected to an accelerometer mounted on the outer housing of the compressor parallel to the crankshaft measured the vibration of the compressor in the loaded operation. The measurement was 16 s long and sampled at 20.833 kHz. Fig. 21 presents the MES calculated over all carrier frequencies. The dominant sixth order

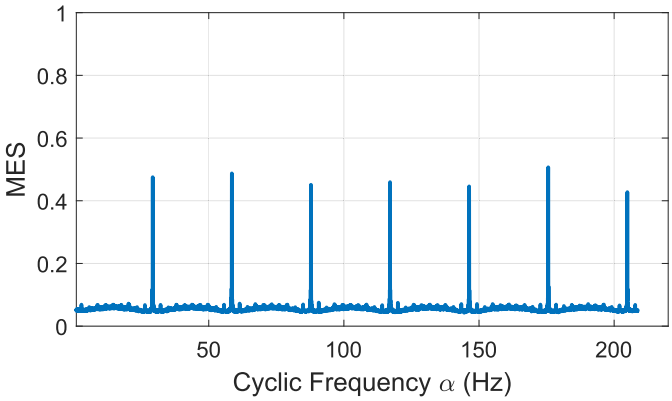

Fig. 21. MES of the loaded Carlyle 06E compressor.

corresponds to the number of activated cylinders. This result provides motivation for the comparison of MES orders, but a more in-depth study of this machine is necessary for statistical verification.

VI. MES-Based Indicator (MESbI) of Activated Cylinders

As discussed in Section IV, for a loaded four-cylinder Carlyle 06D compressor, the fourth-order cyclic frequency is expected to be the dominant component of the MES. For an unloaded compressor, the second-order cyclic frequency is expected to be the dominant component of the MES. Intuition suggests a comparison of the MES at these orders should provide an indicator for the number of activated cylinders. For a vibration measurement and over some range of carrier frequencies F, if the ratio of the MES at the fourth-order cyclic frequency and the MES at the second-order cyclic frequency is greater than one, the fourth order is dominant, and the compressor is likely loaded. If the ratio is less than one, the second order is dominant, and the compressor is likely unloaded. This ratio and simple threshold form a $\text{MESbI}_{4:2}$ of activated cylinders in the machine, where the subscript 4:2 represents MES orders used in the indicator. The number of cylinders of the compressor, unloading details, and physics of the machine motivate the choice of orders for this Carlyle 06D MESbI. Comparison of other orders may be appropriate for other types of reciprocating machines, for example, an MESbI for the Carlyle 06E would include the sixth order. Each MESbI is associated with a range of frequencies F, also referred to here as a region of interest (ROI), over which the MES is calculated. The next paragraphs discuss a method for selecting the ROI.

A new visualization helps determine the ROI for a consistent MESbI. Section IV-C demonstrates the importance F for the MES analysis. Typically, the MES is shown as a 2-D plot such as Fig. 17(b), or the peaks of the MES at harmonics of the shaft frequency are extracted and presented in a bar plot [19]. These visualizations assume a fixed F and are useful after it is determined. A plot of the MESbI versus the upper limit of F, f_{up}, helps select an ROI. For this plot, the bottom limit of F, f_{low}, is set to zero. The visualization is described by

$$\text{MESbI}_{4:2}(f_{\text{up}}) = \frac{S_x^{\langle f_{\text{low}}=0, f_{\text{up}}\rangle}(\alpha_4)}{S_x^{\langle f_{\text{low}}=0, f_{\text{up}}\rangle}(\alpha_2)} \tag{14}$$

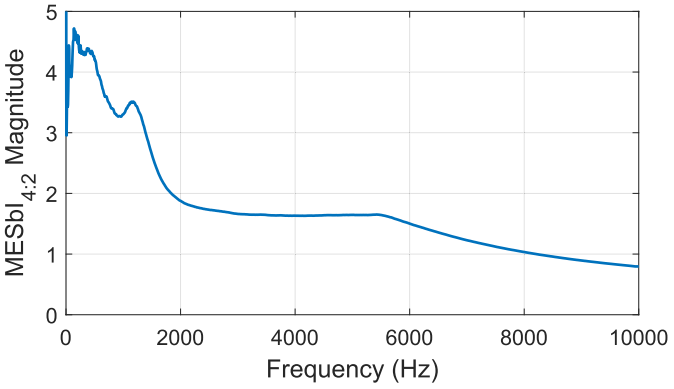

Fig. 22. $\text{MESbI}_{4:2}$ versus f_{up} of the simulated vibration signal of a loaded compressor with uneven responses, uneven modulation, and added high-frequency content.

where $S_x^{\langle f \rangle}$ is the MES of a signal x, f_{up} is the upper limit of F, α_4 is the fourth-order cyclic frequency, and α_2 is the second-order cyclic frequency.

Fig. 22 shows the plot of the $\text{MESbI}_{4:2}$ versus f_{up} for the signal of Fig. 9. The shape of Fig. 22 is explained by inspection of the spectral coherence map in Fig. 12. As f_{up} increases, the MES is evaluated over a larger range of carrier frequencies. For $f_{\text{up}} < 6000$ kHz, the spectral coherence at the fourth-order cyclic frequency $\alpha_4 = 120$ Hz is larger than the spectral coherence at the second-order cyclic frequency $\alpha_2 = 60$ Hz. The ratio of the MESs for this range of upper carrier frequency limit produces a value greater than 1. The peaks and valleys in the $\text{MESbI}_{4:2}$ plot correspond to the addition of peaks and valleys of the spectral coherence magnitude into the MES integral. Past about 6 kHz, the spectral coherence magnitude at the fourth-order cyclic frequency is smaller than the spectral coherence at the second-order cyclic frequency. The addition of this range of carrier frequencies to the MES integral causes the $\text{MESbI}_{4:2}$ to decrease, seen by the negative slope of Fig. 22 starting at about 6 kHz. The value of Fig. 22 at $f_{\text{up}} = 10$ kHz is equal to the division of the MES values of Fig. 17(a) at $\alpha = 120$ Hz and $\alpha = 60$ Hz.

The lower bound f_{low} is equal to zero for Fig. 22, but the selection of f_{low} is an important aspect of the MESbI. For example, $f_{\text{low}} = 6$ kHz and $f_{\text{up}} > f_{\text{low}}$ produce $\text{MESbI}_{4:2}$ with a small value. This choice of f_{low} neglects the range of carrier frequencies where the fourth-order MES is dominant. A systematic selection of F could be done by investigation of the derivative of the $\text{MESbI}_{4:2}$ and choosing areas where the derivative is positive or negative depending on which phenomena are of interest. Plots such as Fig. 22 helped determine the ROIs in Section VII and yielded consistent $\text{MESbI}_{4:2}$ of activated cylinders in the Carlyle 06D refrigeration compressor in shipboard and laboratory test setups.

VII. Experimental Results

This section presents vibration measurements and analysis results from shipboard and laboratory experimental setups. Section VII-A explains the details of the experimental setups. Section VII-B presents a $\text{MESbI}_{4:2}$ for the number of activated cylinders in tested shipboard refrigeration compressors.

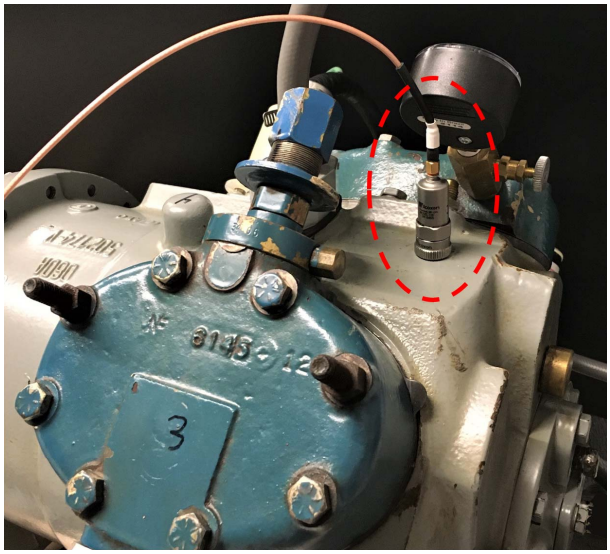

Fig. 23. Accelerometer mounting location.

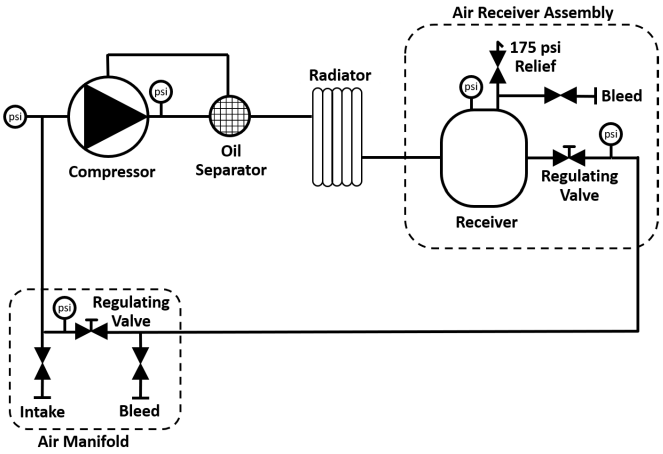

Fig. 24. Schematic of the compressed-air system used for laboratory testing.

Section VII-C presents a $\text{MESbI}_{4:2}$ for the number of activated cylinders of a compressor in a laboratory setup. The results demonstrate the ability of MESbIs with properly selected F to identify activated cylinders in reciprocating machinery.

A. Experimental Setups

Vibration measurements were taken with Wilcoxon's model 728T single-axis 500-mV/g IEPE accelerometer [29] and the custom instrumentation described in [19] and [30]. A wireless connection between the device and a personal computer initiated measurements and transferred data. The accelerometer was mounted with a flat magnet to the discharge port in an orientation perpendicular to the compressor crankshaft, as shown in Fig. 23. The measurements were sampled at 20.833 kHz.

In the shipboard setup, vibration measurements were gathered from two low-temperature refrigerant compressors onboard 270-ft Medium Endurance CG Cutters (WMEC-270s) CGC ESCANABA and CGC SPENCER. Each compressor was a four-cylinder Carlyle model 06D with a mechanical

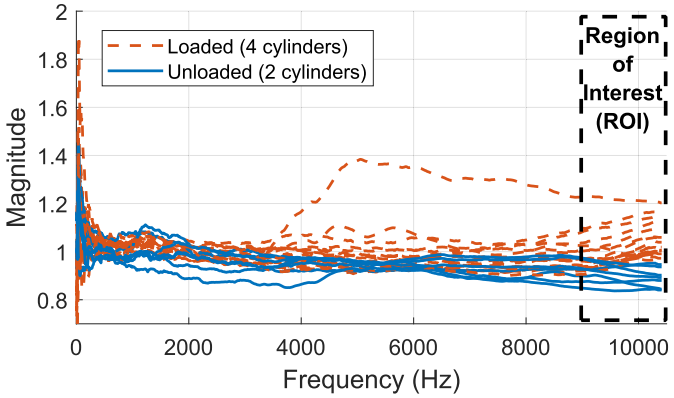

Fig. 25. Shipboard $\text{MESbI}_{4:2}$ versus f_{up} with indicated ROI.

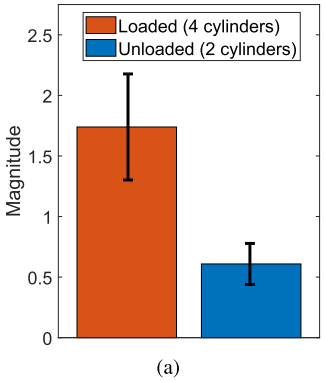

ROI 9 – 10.416 kHz

Loaded		Unloaded
1.558	1.586	0.777
2.694	2.019	0.924
1.492	1.575	0.549
1.289	1.488	0.505
2.240	1.072	0.556
1.744	2.161	0.374
1.324	2.089	0.576
1.105	2.256	
1.874		

(b)

Fig. 26. $\text{MESbI}_{4:2}$ values of shipboard compressor measurements: (a) average values and (b) individual files.

suction-cutoff unloader on one piston pair (head). Each compressor had a dedicated refrigerant loop, condenser, and pair of evaporators. Solenoid supply valves, unloaders, pressure switches, thermal expansion valves, and water regulating valves regulated the system based on cooling demand [31].

A closed-loop compressed-air system constructed in the laboratory simulated the low-temperature refrigeration plant onboard WMEC-270s. The system utilizes the same four-cylinder Carlyle model 06D reciprocating compressor. Fig. 24 shows a schematic of the compressed-air laboratory system. An air manifold controls the volume of air introduced to the system until the desired system pressure is reached. Once this system pressure is reached, the air manifold bleed and intake valves are closed and form a closed loop. The air receiver assembly regulating valve controls compressor suction pressure.

B. Shipboard Files

Twenty-four vibration measurements from shipboard compressors with a known operating state were acquired. In both shipboard and laboratory setups, compressor unloaders were manually manipulated to achieve a known number of activated cylinders (loading condition). Fig. 25 presents the $\text{MESbI}_{4:2}$ versus f_{up} for each of the 24 shipboard measurements. The 17 dashed lines are loaded measurements, and the seven solid lines are unloaded measurements.

All four pistons reciprocate regardless of operating state, but compression forces, valve action, and passage of discharge gas are distinct for loaded and unloaded operation. For the shipboard compressors, these changes are most significant in the $\text{MESbI}_{4:2}$ at frequencies greater than 9 kHz. That is, above 9 kHz, the fourth-order:second-order MES ratios in Fig. 25 tend to increase for loaded measurements and decrease for unloaded measurements. Compressor vibration is a complex combination of factors, and given the unknown condition of these compressors, it is difficult to ascribe all peaks and valleys of the MES to specific causes. However, for the measured files, $\text{MESbI}_{4:2}$ with an ROI of 9–10.416 kHz provides a consistent indicator of compressor loading state. Sampling frequency and mounting configuration constrain the upper bound of the ROI (10.416 kHz is the Nyquist frequency). The bars in Fig. 26(a) show the average $\text{MESbI}_{4:2}$ values for the shipboard files. The average $\text{MESbI}_{4:2}$ was 1.74 for the loaded files and 0.61 for the unloaded files. The bounds around the top of the bars represent one standard deviation above and below the mean. The standard deviation of the $\text{MESbI}_{4:2}$ was 0.44 for the loaded files and 0.17 for the unloaded files. Fig. 26(b) shows the $\text{MESbI}_{4:2}$ values for each measured file. There is separation between the $\text{MESbI}_{4:2}$ values, and the $\text{MESbI}_{4:2}$ correctly classifies loaded and unloaded operations for all files.

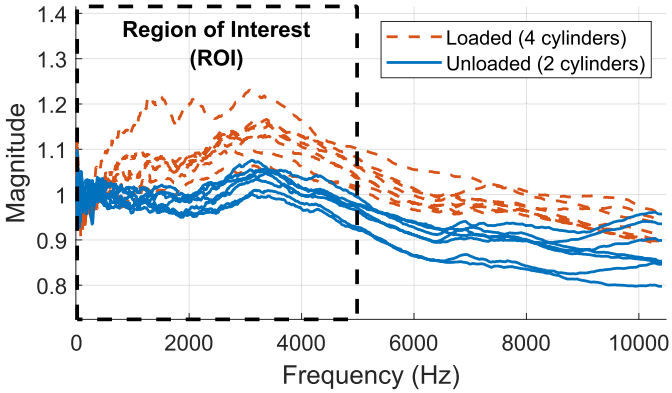

Fig. 27. Laboratory $\text{MESbI}_{4:2}$ versus f_{up} with indicated ROI.

C. Laboratory Files

Fifteen vibration measurements from the laboratory compressor with a known operating state were acquired. Fig. 27 presents the $\text{MESbI}_{4:2}$ for each of the 15 laboratory measurements. The eight dashed lines represent loaded measurements, and the seven solid lines represent unloaded measurements. Overall, the laboratory $\text{MESbI}_{4:2}$ in Fig. 27 has a different nature than the shipboard $\text{MESbI}_{4:2}$ in Fig. 25. Although the same model of the compressor was used, there are significant differences between the laboratory compressed-air system and the shipboard refrigerant system. In addition, the mechanical health (condition) of each compressor affects the MES [4], [19]. For the laboratory compressor, there are notable differences between loaded and unloaded ratios, especially below 5 kHz. For the measured files, $\text{MESbI}_{4:2}$ with an ROI of 0–5.0 kHz provides a consistent indicator of compressor loading state. The bars in Fig. 28(a) show the average $\text{MESbI}_{4:2}$ values for the laboratory files. The average $\text{MESbI}_{4:2}$ was

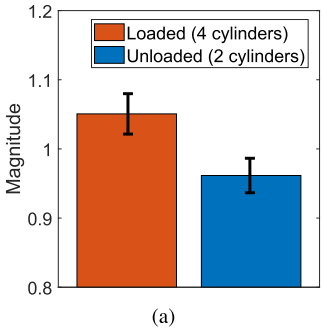

(a)

ROI 0 – 5.0 kHz

Loaded	Unloaded
1.018	0.977
1.101	0.962
1.064	0.995
1.080	0.970
1.086	0.922
1.039	0.928
1.036	0.977
1.059	

(b)

Fig. 28. $MESbI_{4:2}$ values of laboratory compressor measurements: (a) average values and (b) individual files.

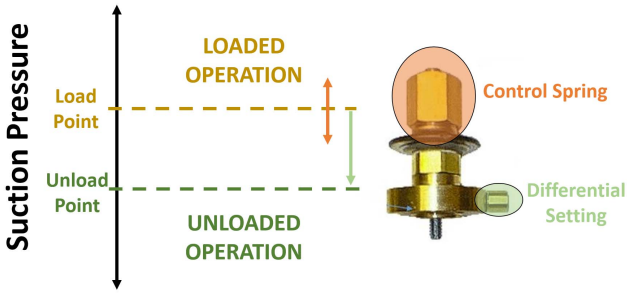

Fig. 29. Mechanical control valve adjustment settings.

1.05 for the loaded files and 0.96 for the unloaded files. The bounds around the top of the bars represent one standard deviation above and below the mean. The standard deviation of the $MESbI_{4:2}$ was 0.029 for the loaded files and 0.025 for the unloaded files. Fig. 28(b) shows the $MESbI_{4:2}$ values for each measured file. Compared to the shipboard data, there is not as distinct of a separation between the loaded and unloaded laboratory files, but the $MESbI_{4:2}$ with an ROI of 0–5 kHz still correctly classifies loaded and unloaded operation for all files.

VIII. Discussion

A. Measurement Uncertainty

Many phenomena contribute to the measured vibration signal of mechanical machinery. For example, the type of data acquisition circuitry, sensor topology and mounting location, and environmental variables, such as temperature, all influence the vibration signature. The exact or "true" vibration signal is never measured in practice but rather a signal altered by the characteristics of the measurement setup and other external factors.

To limit measurement uncertainty in Section VII, the same measurement hardware mounted at the same location across the compressors collected the vibration signals. The sets of loaded and unloaded measurements were from steady-state operation (no sudden changes in load) and grouped by load state but included files with various system temperatures and pressures. As a general best practice, as far as is practical, all contributing factors should be monitored, recorded, and compared across like values. Given the mix of temperatures and pressures for the measurements, the separation of the results in Section VII-C demonstrates that, for this machine, the MESbI primarily depends on load state, a desirable feature for a load-state indicator. Deviation about the average values would likely decrease if the experiment only considered files with certain system temperatures and pressures.

B. Continuous Commissioning

Commissioning procedures validate and tune the operation of new machinery and systems. Continuous commissioning refers to system adjustments made throughout the life cycle of equipment based on machine health and system requirements. Nonintrusive monitoring systems provide valuable insights for continuous commissioning. This section considers the continuous commissioning of refrigerant compressors' capacity control valves.

Typically, capacity control valves are set by a heuristic process based on technician experience. The initial set point of a capacity control valve may not fully represent system demand or operating conditions and may require periodic adjustments. The unloader's control spring set point is adjustable from 0 to 12 turns from its bottom stop. Fig. 29 shows the effect of the control spring and differential setting on compressor loading setpoints. The dashed lines are the hysteresis bands of the capacity control valve. A set point zero turn from the bottom stop (zero visible threads) corresponds to a fully compressed control spring and a load point of 86-psi suction pressure. A set point of 12 turns from the bottom stop (12 visible threads) corresponds to a fully uncompressed control spring and a load point of 0-psi suction pressure. For an R-134A system with a nominal discharge pressure of 150 psi, the control spring set point should be 10.5–12 turns.

Fig. 30(a) shows the capacity control valve of a brand-new compressor. The manufacturer set point of a new compressor is four turns. The control spring set point varies significantly across WMEC-270 refrigeration plants. For example, Fig. 30(b) and (c) shows control spring set points on CGC BEAR with six and 11 turns, respectively. The 11-turn set point is within the recommended range, but the six-turn set point will result in perpetual unloaded compressor operation regardless of cooling demand. A continuous commissioning process aided by nonintrusive vibration monitoring could aid capacity control valve set point procedures and extend the useful life of shipboard compressors.

Continuous commissioning provides a structured approach to capacity control valve setting and, however, requires knowledge of suction pressure and compressor load state. Vibration measurement and the techniques of Section VII provide a means of determining compressor load state. To employ the techniques, calibration is required. First, an operator acquires vibration measurements with the control spring fully compressed and uncompressed. A fully compressed control spring guarantees loaded operation. A fully uncompressed control spring guarantees unloaded operation. Multiple measurements (as many as practical) in each loading state across different operating pressures and with various accelerometer mounting locations would provide the best results and intuition for how the MES varies in different scenarios. For all measurements,

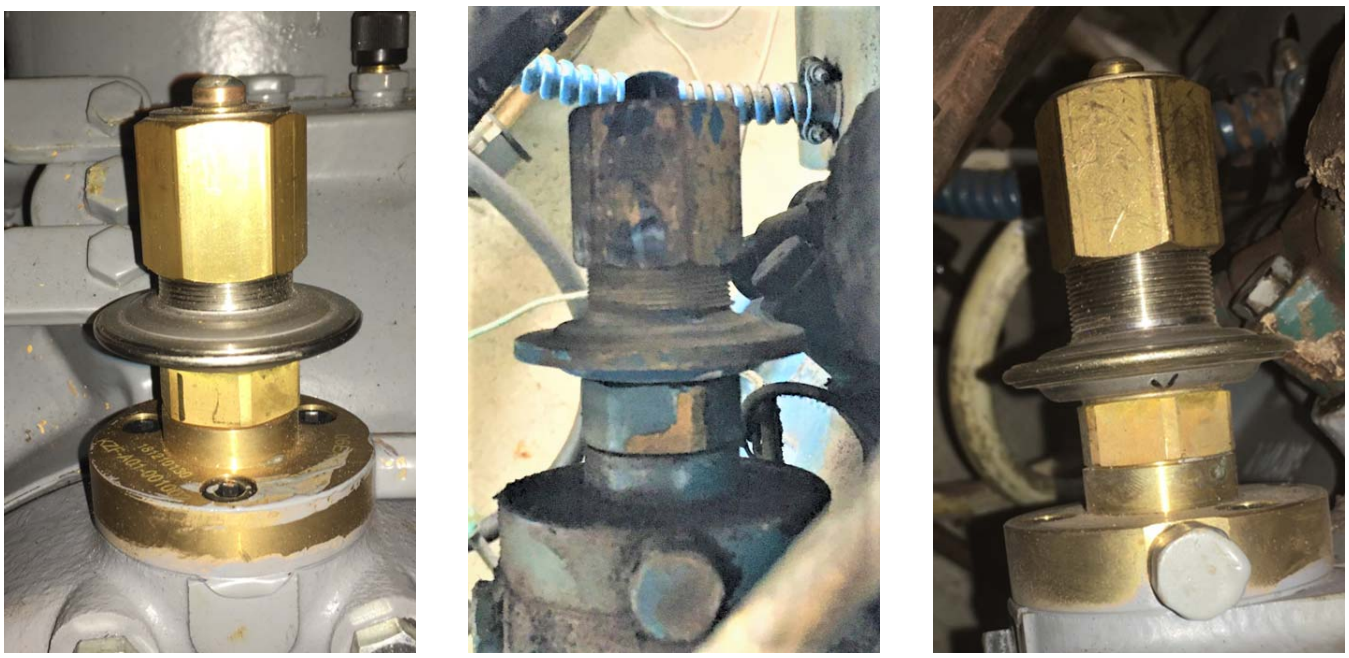

(a) (b) (c)

Fig. 30. Various capacity control valve set points found onboard WMEC-270s: (a) manufacturer set point (four turns), (b) six-turn set point observed on CGC BEAR, and (c) 11-turn set point observed on CGC BEAR.

the operator calculates the MES. The operator then investigates the MESbI (with orders determined from machine physics) and chooses the accelerometer mounting location and ROI that provide the most consistent indication of loading condition, i.e., an MESbI with distinct values for each operating state and small deviation from those values across the files. With the ROI and mounting location determined, the calibration is complete. The calibrated MESbI can identify the compressor loading state of a healthy machine, help tune control spring set points, and confirm the operating state with suction pressure measurements.

IX. Conclusion

This article demonstrates the utility of cyclostationary signal processing for the detection of activated cylinders in reciprocating machines. Simulations in Section IV show how simple physics-based signal models provide intuition for signal-processing tools and diagnostic approaches. This section could guide technicians and engineers in their own applications. Section V demonstrates other types of equipment with potentially interesting MES signatures and motivates the comparison of the relative magnitudes of MES orders. An experimental study with a four-cylinder Carlyle 06D compressor presents an MESbI that consistently classifies the loading condition in both laboratory and shipboard environments. The proposed activated-cylinder detection method requires calibration with vibration measurements with a known number of activated cylinders. Section VIII-B discusses a potential application for continuous commissioning of reciprocating compressor unloader capacity control valves. In this case, calibration is simply turning a set-point nut and measuring the vibration for known loading states. A well-tuned set point aided by the MESbI would likely increase compressor lifetime. More generally, the proposed method could diagnose cylinder faults in reciprocating machines, such as misfires or blown values.

References

[1] C. B. Brusso, "The end of coal-fired power generation in Chicago [history]," *IEEE Ind. Appl. Mag.*, vol. 27, no. 3, pp. 8–15, Jun. 2021.

[2] L. do Nascimento Cervelin, D. H. S. Arruda, R. C. C. Flesch, and J. N. Scussel, "Measurement of the instantaneous in-cylinder pressure of reciprocating compressors using the connecting rod strain," *IEEE Instrum. Meas. Mag.*, vol. 23, no. 7, pp. 34–39, Oct. 2020.

[3] A. P. Lindahl et al., "Nonintrusive load monitoring of variable speed drive cooling systems," *IEEE Access*, vol. 8, pp. 211451–211463, 2020.

[4] L. Huchel, J. Helsen, P. A. Lindahl, and S. B. Leeb, "Diagnostics for periodically excited actuators," *IEEE Trans. Instrum. Meas.*, vol. 69, no. 7, pp. 4145–4153, Jul. 2020.

[5] M. Corno, L. D'Avico, S. Marelli, M. Galvani, and S. M. Savaresi, "Predictive cylinder deactivation control for large displacement automotive engines," *IEEE Trans. Veh. Technol.*, vol. 68, no. 10, pp. 9554–9563, Oct. 2019.

[6] Y. Nishibe, Y. Nonomura, K. Tsukada, M. Takeuchi, M. Miyashita, and K. Ito, "Determination of engine misfiring using magnetoelastic torque sensor," *IEEE Trans. Instrum. Meas.*, vol. 47, no. 3, pp. 760–765, Jun. 1998.

[7] P. Azzoni and M. Marseguerra, "Assessment of the potential of a Wiener–Hilbert filter for automatic diagnosis of spark ignition engine faults," *Mech. Syst. Signal Process.*, vol. 9, no. 2, pp. 119–128, Mar. 1995.

[8] P. Charles, J. K. Sinha, F. Gu, L. Lidstone, and A. D. Ball, "Detecting the crankshaft torsional vibration of diesel engines for combustion related diagnosis," *J. Sound Vib.*, vol. 321, nos. 3–5, pp. 1171–1185, 2009.

[9] K. Wu, Z. Liu, Q. Ding, F. Gu, and A. Ball, "Torsional vibration responses of the engine crankshaft-gearbox coupled system with misfire and breathing slant crack based on instantaneous angular speed," *Mech. Syst. Signal Process.*, vol. 173, Jul. 2022, Art. no. 109052.

[10] J. Chen and R. B. Randall, "Improved automated diagnosis of misfire in internal combustion engines based on simulation models," *Mech. Syst. Signal Process.*, vols. 64–65, pp. 58–83, Dec. 2015.

[11] J. Antoni, J. Daniere, and F. Guillet, "Effective vibration analysis of IC engines using cyclostationarity. Part I—A methodology for condition monitoring," *J. Sound Vibrat.*, vol. 257, no. 5, pp. 815–837, Nov. 2002.

[12] J. Antoni, J. Daniere, F. Guillet, and R. B. Randall, "Effective vibration analysis of IC engines using cyclostationarity. Part II—New results on the reconstruction of the cylinder pressures," *J. Sound Vibrat.*, vol. 257, no. 5, pp. 839–856, 2002.
[13] R. B. Randall, *Vibration-Based Condition Monitoring: Industrial, Aerospace and Automotive Applications*. Hoboken, NJ, USA: Wiley, 2011.
[14] J. Antoni, "Cyclostationarity by examples," *Mech. Syst. Signal Process.*, vol. 23, no. 4, pp. 987–1036, May 2009.
[15] C. Luo, Z. Mo, and Q. Miao, "Cyclic harmonic ratio defined in squared envelope spectrum and log-envelope spectrum for gearbox fault diagnosis," *IEEE Trans. Instrum. Meas.*, vol. 69, no. 12, pp. 9568–9577, Dec. 2020.
[16] R.-B. Sun, F.-P. Du, Z.-B. Yang, X.-F. Chen, and K. Gryllias, "Cyclostationary analysis of irregular statistical cyclicity and extraction of rotating speed for bearing diagnostics with speed fluctuations," *IEEE Trans. Instrum. Meas.*, vol. 70, pp. 1–11, 2021.
[17] D. Abboud and J. Antoni, "Order-frequency analysis of machine signals," *Mech. Syst. Signal Process.*, vol. 87, pp. 229–258, Mar. 2017.
[18] A. Mauricio, W. A. Smith, R. B. Randall, J. Antoni, and K. Gryllias, "Improved envelope spectrum via feature optimisation-gram (IESFOgram): A novel tool for rolling element bearing diagnostics under non-stationary operating conditions," *Mech. Syst. Signal Process.*, vol. 144, Oct. 2020, Art. no. 106891.
[19] L. Huchel, T. C. Krause, T. Lugowski, S. B. Leeb, and J. Helsen, "Chasing the cut: A measurement approach for machine tool condition monitoring," *IEEE Trans. Instrum. Meas.*, vol. 70, pp. 1–10, 2021.
[20] W. A. Gardner, *Statistical Spectral Analysis: A Nonprobabilistic Theory*. Englewood Cliffs, NJ, USA: Prentice-Hall, 1988.
[21] W. A. Gardner, *Introduction to Random Processes With Applications to Signals and Systems*. New York, NY, USA: Macmillan, 1986.
[22] A. V. Oppenheim and R. W. Schafer, *Discrete Time Signal Processing*. London, U.K.: Pearson, 2013.
[23] *Carlyle Compressor—Electronic Drawings*. Accessed: 2022. [Online]. Available: https://www.carlylecompressor.com/support/electronic-drawings/
[24] P. C. Hanlon, *Compressor Handbook*, 1st ed. New York, NY, USA: McGraw-Hill, 2001.
[25] *Instructions #99Ta516175B—Capacity Control Accessory Packages (Pressure & Electronic)*. Accessed: 2022. [Online]. Available: https://www.shareddocs.com/hvac/docs/2002/Public/06/99TA516175Bcw.pdf
[26] N. J. Trout and R. J. Kolodzie, "Reciprocating compressor valve condition monitoring using image-based pattern recognition," in *Proc. Annu. Conf. Prognostics Health Manage. Soc.*, 2016, pp. 1–10.
[27] A. V. Oppenheim, S. A. Willsky, and S. H. Nawab, *Signals and Systems*. Upper Saddle River, NJ, USA: Prentice-Hall, 1997.
[28] J. Antoni, G. Xin, and N. Hamzaoui, "Fast computation of the spectral correlation," *Mech. Syst. Signal Process.*, vol. 92, pp. 248–277, Aug. 2017.
[29] *Wilcoxon Research—Model 728T High Sensitivity, Low Noise Accelerometers*. Accessed: 2022. [Online]. Available: https://buy.wilcoxon.com/
[30] L. Huchel, T. C. Krause, S. B. Leeb, and J. Helsen, "Stretched sensing strategies for IEPE," *IEEE Trans. Instrum. Meas.*, vol. 70, pp. 1–10, 2021.
[31] H. D. McGeorge, *Marine Auxiliary Machinery*, 7th ed. Oxford, U.K.: Butterworth-Heineman, 1995.

Thomas C. Krause (Graduate Student Member, IEEE) received the B.S. degree in electrical engineering from Purdue University, West Lafayette, IN, USA, in 2019, and the M.S. degree in electrical engineering and computer science from the Massachusetts Institute of Technology, Cambridge, MA, USA, in 2021, where he is currently pursuing the Ph.D. degree in electrical engineering and computer science.

Devin W. Quinn received the M.S. degree in mechanical engineering from the Massachusetts Institute of Technology, Cambridge, MA, USA, in 2022.

He was previously stationed as a Damage Control Officer aboard USCGC DILIGENCE and an Engineer Officer onboard USCGC ESCANABA. He is currently a Lieutenant Commander with the United States Coast Guard, Alameda, CA, USA.

Łukasz Huchel received the B.Sc. degree in electrical power engineering from the Silesian University of Technology, Gliwice, Poland, in 2013, the M.Sc. degree from the Department of Electrical Engineering and Computer Science (EECS), Masdar Institute of Science and Technology, Abu Dhabi, United Arab Emirates, in 2015, and the Ph.D. degree from the Massachusetts Institute of Technology, Cambridge, MA, USA, in 2021.

He is currently with Enphase Energy, Austin, TX, USA.

Steven B. Leeb (Fellow, IEEE) received the Ph.D. degree from the Massachusetts Institute of Technology (MIT), Cambridge, MA, USA, in 1993.

He has served as a Commissioned Officer in the USAF reserves. He has been a member of the M.I.T. Faculty, Department of Electrical Engineering and Computer Science, Massachusetts Institute of Technology, since 1993. He also holds a joint appointment in the Department of Mechanical Engineering, MIT. He is the author or a coauthor of over 200 publications and 20 U.S. patents in the fields of electromechanics and power electronics.